The latest Post-Variscan fluids in the Spanish Central System: evidence from fluid inclusion and stable isotope data

Tomás Martín Crespo[a,*], Antonio Delgado[b,1], Elena Vindel Catena[a], José Angel López García[a], Cécile Fabre[c]

[a]*Departamento de Cristalografía y Mineralogía, Facultad de Ciencias Geológicas, Complutense University, 28040 Madrid, Spain*
[b]*Departamento de Ciencias de la Tierra y Química Ambiental, Estación Experimental del Zaidín (CSIC), 18008 Granada, Spain*
[c]*CREGU-G2R, BP 23, 54501 Vandeouvre les Nancy, France*

Abstract

The Spanish Central System has been subjected to repeated fluid incursions, which were responsible for a variety of mineralizing episodes including W–Sn, Cu–Zn–Pb–As–(Ag), F–Ba and barren quartz veins. These hydrothermal fluids occurred over a 200 Ma time period and the latest hydrothermal event is recorded in barren quartz veins. This study is a multidisciplinary approach leading to the characterization of the hydrothermal fluids preserved in barren quartz veins, which are spatially but not temporally related to Hercynian upper crustal granites. The veins were dated by the $^{39}Ar/^{40}Ar$ method, and the fluids were examined using petrographic, microthermometric, chemical and isotopic methods. Fluid inclusions in barren quartz veins indicate that two fluids were related to this hydrothermal event. The main part of the quartz veins were formed from an early low salinity (<1 wt% NaCl) H_2O–NaCl fluid. This fluid was trapped at around 270 ± 25 °C and 0.1–1 kbar under sublithostatic to hydrostatic conditions. $\delta^{18}O$ (−9 to 2‰) and δD (−70 to −34.5‰) values indicate a meteoric origin for water, with significant water/rock interactions. The latest H_2O–NaCl–$CaCl_2$ fluid is found in two types of fluid inclusions: a primary liquid–vapour type (16–24 wt% NaCl and 1–12 wt% $CaCl_2$) and secondary hypersaline type (7–15 wt% NaCl and 21–27 wt% $CaCl_2$). Significant Li concentrations in this fluid were confirmed. This late Ca-bearing fluid formed quartz crystals in the central part of the veins, and was trapped at 70–140 °C, at a maximum pressure of 0.5 kbar. The low $\delta^{18}O$ (−20 to −6‰) and δD (−137 to −116‰) values suggest a meteoric origin for this fluid, however its high salinity probably requires a source from Triassic evaporite basins located in the NE tip of the Spanish Central System. Anomalously low isotopic values have been previously reported from kaolinites of Lower Cretaceous age. Anomalous climatic conditions during the Cretaceous appear to be the main reason to explain this very negative meteoric water. Strong isotopic depletion in meteoric water has been observed in modern areas with monsoonal climates. The hydrothermal evolution of barren quartz veins in the Spanish Central System is comparable to other hydrothermal Post-Variscan events in central and south-western Europe related to the opening of the North-Atlantic during Cretaceous time.

Keywords: Fluid inclusions; Stable isotopes; Hydrothermal fluids; Post-Variscan; Spanish Central System

1. Introduction

The Spanish Central System has been subjected to repeated fluid incursions, which are responsible for different types of granite-hosted and metamorphic-hosted mineralization: W–Sn, Cu–Zn–Pb–As(Ag) sulphides, F–Ba and barren quartz veins. Thus, the Spanish Central System offers a good opportunity to analyse a variety of hydrothermal fluids, which may be compared to other hydrothermal Post-Variscan events in Europe. These hydrothermal fluids span a time interval of around 200 Ma. Fluids trapped in the barren quartz veins represent the latest hydrothermal event (Caballero et al., 1992; Tornos, Delgado, Casquet, & Galindo, 2000; Vindel, Lopez, Martín Crespo, & García, 2000). Tungsten base-metal transport were related to aqueous-carbonic fluids (García, Vindel, & López García, 1999a,b; Vindel, Lopez, Boiron, Cathelineau, & Prieto, 1995), fluorite–barite ores to aqueous fluids (Galindo, Tornos, Darbyshire, & Casquet, 1994; Tornos, Casquet, Locutura, & Collado, 1991) and later barren quartz veins to $CaCl_2$ brines (Martín Crespo, López García, Banks, Vindel, & García, 1999). This study encompasses for the first time the whole evolution of hydrothermal events. Ca-bearing fluids have not been previously clearly defined in

* Corresponding author. Fax: +34-91-394-48-72.
E-mail addresses: tmartin@geo.ucm.es (T. Martín Crespo), antodel@eez.csic.es (A. Delgado), evindel@geo.ucm.es (E. Vindel Catena), jangel@geo.ucm.es (J.A. López García).
[1] Fax: +34-95-812-96-00.

the Spanish Central System, and could be compared to the Ca-rich brines found in other Post-Variscan hydrothermal mineralizations in Europe (Behr & Gerler, 1987; Behr, Horn, Frentzel-Beyme, & Reutel, 1987; Canals & Cardellach, 1993; Charef & Sheppard, 1988; Lodemann et al., 1998; Muchez & Sintubin, 1998; Muchez, Slobodnik, Viaene, & Keppens, 1995; Munoz, Boyce, Courjault-Rade, Fallick, & Tollon, 1994, 1999; O'Connor, Högelsberger, Feely, & Rex, 1993; O'Reilly, Jenkin, Feely, Alderton, & Fallick, 1997; Wilkinson, Jenkin, Fallick, & Foster, 1995). Fluid migration during Mesozoic time in the Spanish Central System comprise a flow system involving meteoric waters that increased in salinity because of interaction with evaporitic-bearing sequences.

2. Geological setting

The Spanish Central System is a northeast trending mountain range located in the inner zone of the Hercynian Belt of Spain. Its central part, the so-called 'Sierra de Guadarrama', consists of granitoids and high to medium grade metamorphic rocks, mostly pre-Hercynian orthogneisses and some pre-Ordovician metasedimentary rocks. Scattered relicts of small Permian detrital basins, and of a Triassic and Jurassic cover, are also preserved in the northeast of the Spanish Central System. Late Hercynian granitoids were emplaced from 345 to 285 Ma (Casillas, Vialette, Peinado, Duthou, & Pin, 1991; Ibarrola et al., 1987; Pérez del Villar, Crespo, Pardillo, Pelayo, & Galán, 1996a; Pérez del Villar et al., 1996b; Vialette, Bellido, Fúster, & Ibarrola, 1981; Villaseca, Eugercios, Snelling, Huertas, & Castellón, 1995) after the main Hercynian orogeny. The granitoids are mostly peraluminous monzogranites and leucogranites, with minor intrusions of more mafic composition. The main groups of granitoids generate typical contact aureoles in the surrounding wall rocks indicating a high emplacement level, between 5 and 8 km depth (Villaseca, Barbero, & Rodgers, 1998). The Sierra de Guadarrama has experienced numerous fluid–rock interaction events. Mineralization is of minor economic importance, although a large number of mineralised veins accompanied by hydrothemal alteration occur throughout the batholith and country rocks (Vindel et al., 1995). The oldest hydrothermal event (300–290 Ma) was associated with veins containing wolframite and sulphides in greisenized granites, whereas barren quartz veins are the most recent event. An age of 100.6 ± 4.3 Ma was obtained from a granite-hosted barren quartz vein by K–Ar dating of sericite from phyllic alteration (Caballero et al., 1992).

3. Barren quartz veins

A large number of veins have been identified throughout the granitic (Colmenarejo, Cerceda, Manzanares el Real, La Cabrera) and metamorphic outcrops (Colmenarejo, Colmenar Viejo) of Sierra de Guadarrama (Fig. 1). Their essential features are given in Table 1.

3.1. Granite-hosted barren quartz veins

These veins range in thickness from 0.3 to 5 m, have strike lengths of up to 2 km and have subvertical dips. The two most frequent strike directions are N20°E and N110°E, which follow the main extensional directions between Lower and Upper Cretaceous cover (Alonso & Mas, 1982).

Host rock features and the main characteristics of the veins are outlined below:

Colmenarejo (COL): barren quartz veins crosscut the Zarzalejo–Valdemorillo biotitic monzogranite. The texture of this granite is typically hypidiomorphic and equigranular, however, a porphyritic facies with a medium-grained matrix has also been observed. The veins are located in the SE of the area and comprise a group of 10 N20°E veins. Several later fractures striking E–W have affected the quartz veins.

Cerceda (CER): veins occur throughout two granite types, a fine-grained leucogranite and a porphyritic coarse-grained monzogranite (El Cardín type; Villaseca et al., 1998). Four quartz veins have been recognised along the contact between the two granites, which display a predominantly strike N–S.

The Manzanares el Real (MAN) quartz vein also crosscuts the El Cardín granite (Villaseca et al., 1998). A single N116°E barren quartz vein has been recognised in this area.

The La Cabrera (CAB) massif represents the eastern-most granitic intrusion in the Spanish Central System. It comprises of several varieties of granite. The main facies comprises medium to coarse-grained biotitic granites and monzogranites with subordinate porphyritic varieties. Medium to fine-grained, biotitic, highly evolved leucogranites are related to this main facies (Bellido et al., 1981). The studied quartz vein occur in the biotitic granite, striking N20°E, and is located in the SW part of the batholith.

Three morphological and textural types of quartz can be distinguished in most of the veins: (1) massive quartz (QI) at the vein margins. Suitable fluid inclusions for microthermometric analyses (>5 μm) are not recognised in this type of quartz; (2) central part of clear quartz crystals (QII) located in the centre of the veins, and (3) margin of QII crystal (QIII). Both QII and QIII appear in vug cavities and contain abundant fluid inclusions. Hydrothermal muscovite, minor amounts of fluorite and iron oxides have been recognised between quartz crystals (Table 1).

Hydrothermal alteration is restricted to the proximity of the lodes (around 0.5 m width), and is poorly developed. Muscovitization and chloritization are the usual and most

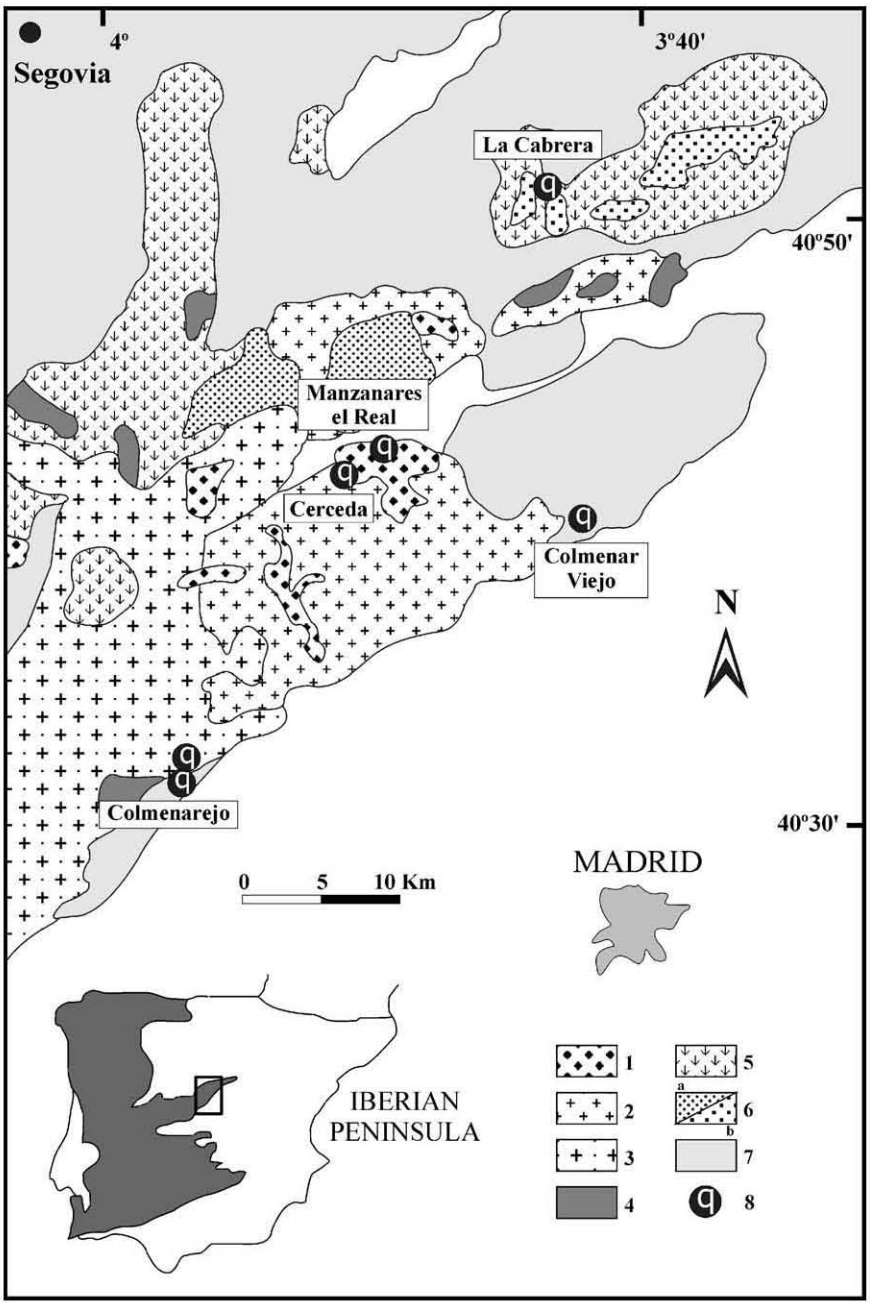

Fig. 1. Simplified map of the studied area showing the barren quartz vein locations. Legend: (1) leucogranite, (2) coarse-grained monzogranite, (3) porphyritic monzogranite, (4) not assigned granite, (5) monzogranite, (6a) coarse-grained leucogranite, (6b) leucogranite, (7) metamorphic rock, (8) barren quartz vein (after Villaseca et al., 1998).

important alterations. Muscovitization is generated by alteration of feldspars, while chloritization is restricted to the alteration of biotites within the granites.

3.2. Gneiss-hosted barren quartz veins

Gneiss-hosted quartz veins (Colmenarejo and Colmenar Viejo) crosscut pre-Hercynian augen orthogneisses. They show a similar structural setting, paragenesis and wall-rock alteration to the granite-hosted veins. At Colmenarejo, the N20°E veins cut both a monzogranite and a augen orthogneiss. Brecciation of wallrock and veins is characteristic, showing typically massive veins and crosscutting microveins, like stockworks. Brecciated fragments of wall-rock occur in several veins. Only QI and QII quartz types are recognised in these veins. Hydrothermal alteration is restricted to a narrow zone (~10 cm) adjacent to the veins and is characterised by muscovitization of feldspars. Five barren quartz veins striking N20–40°E have been studied at Colmenar Viejo. Silicification and muscovitization were recognised as hydrothermal alterations.

Table 1
Characteristic features of the barren quartz veins

Vein location	Strike/dip	Thickness (m)	Length (m)	Host rock	Alteration	Mineralogy
Colmenarejo	N20°E 65°W/subvertical	1–5	0.3–2	Biotitic monzogranite	Chloritization, muscovitization	Quartz, muscovite
Colmenarejo	N–S/N20°E 50°W/subvertical	1–2	0.3–0.8	Augen orthogneiss	Brecciation of wallrock, muscovitization	Quartz, muscovite
Cerceda	N–S subvertical	0.5–4	0.5–2	Leucogranite monzogranite	Chloritization, muscovitization, oxidation	Quartz, muscovite, fluorite
Manzanares el Real	N115°E subvertical	0.5–1	≈ 0.4	Leucogranite	Chloritization, muscovitization, oxidation	Quartz, micas, Fe oxide
La Cabrera	N–S/N20°E subvertical	0.5–2	0.5–0.8	Biotitic monzogranite	N.R.	Quartz, muscovite
Colmenar Viejo	N20–40°E subvertical	0.3–4	0.1–0.4	Augen orthogneiss	Silicification, muscovitization	Quartz

4. Analytical methods

A microthermometric study (~1000 inclusions from 44 samples) was carried out on doubly polished wafers (<300 μm in thickness) using a Linkam THMSG 600 heating–freezing stage (MacDonald & Spooner, 1981). The stage was calibrated with melting-point of solid standards at $T > 25$ °C, and natural and synthetic inclusions at $T < 0$ °C. The rate of heating was monitored in order to get an accuracy of ±0.2 °C during freezing, ±1 °C when heating over the 25–400 °C range, and ±4 °C over the 400–600 °C range. Salinity of H_2O–NaCl inclusions, expressed as equivalent weight percent NaCl, was calculated from microthermometric data using equations from Bodnar (1993). Salinity and composition of H_2O–NaCl–$CaCl_2$ inclusions was established from ice, hydrohalite and halite melting temperatures using a Microsoft Excel Add-in developed by J. Naden (Naden, 1996).

P–T properties for the H_2O–NaCl–$CaCl_2$ system are not available, but data from Zhang and Frantz (1987) for the H_2O–NaCl system can be used to approximate the inclusion isochores.

Determination of ion ratios in individual fluid inclusions was done by Laser Induced Breakdown Spectroscopy (LIBS), coupling laser ablation with an optical emission spectrometer at CREGU, Nancy. Recent developments using LIBS, previously described by Boiron et al. (1991, 1997), Fabre, Boiron, Dubessy, and Moissette (1999) and Moissette et al. (1997), have shown that this method can be adapted for the analysis of the ion content in individual fluid inclusions. A 5 ns laser pulse is delivered by a Nd-YAG laser (266 nm) and focused onto the sample through a Cassegrain objective. A plasma is created by the interaction of the laser and matter. Emission lines of elements present in the plasma are directly analysed by an optical emission spectrometer equipped with a pulsed and gated multichannel detector. The intensity of the emission lines is proportional to the concentration of the elements. The repeatability of LIBS for net intensity ratios is around 10 and 20% for glasses and fluid inclusions, respectively (Fabre et al., 1999). Such results are quite acceptable for the validation of the analytical data. The detection limits are calculated for major elements in fluid inclusions and are for Na and Li 10 ppm, Ca 20 ppm and K 750 ppm. These detection limits are those required for the determination of ions in a majority of fluid inclusions.

Bulk crush-leach analysis was performed on samples (between 0.5 and 1 g) prepared and analysed using the procedures set out in Bottrell, Yardley, and Buckley (1988), and modified by Yardley, Banks, Bottrell, and Diamond (1993). The anions Cl and Br were analysed by ion chromatography on double distilled water leaches using a Dionex 4500I HPLC. Na was determined on the same solution leached with an acidified $LaCl_3$ solution by Flame Emission Spectroscopy (FES).

Irradiation and stepwise heating of micas was done

according to Kamber, >Blenkinsop, Villa, and Dahl (1995). 10 mg of mica were handpicked to achieve visual purity of ~100%. The selected sample was irradiated in the Risø reactor (Denmark), and step-heated in a double-vacuum resistance oven connected to a MAP 215-50B mass spectrometer. The analyses were carried out at the Mineralogisches Institut, Bern (Switzerland).

Thermal decrepitation was chosen as the method for extracting fluid inclusions from quartz for the hydrogen isotope analyses. Values of δD_{fluid} were determined using the uranium technique, with a similar methodology to that described by Godfrey (1962). Samples were degassed overnight by heating at 70 °C under high vacuum. The platinum crucible was then heated (by a radio-frequency induction furnace) to approximately 1200 °C. The released water was converted to hydrogen by passing over uranium metal at about 800 °C. δO^{18} was determined in quartz (10–15 mg) reacting with a stoichiometric excess of ClF_3 at 650 °C for 12 h (Borthwick & Harmon, 1982; Vennemann & Smith, 1990). Released oxygen was converted to CO_2 by reaction with a hot platinized graphite rod (Clayton & Mayeda, 1963). The isotope ratios were measured in a Finnigan MAT 251 mass spectrometer. Commercial CO_2 was used as the internal standard for the oxygen analyses of silicates contrasted with the V-SMOW, SLAP and GIPS water standards, giving a value of $\delta^{18}O = +9.6 \pm 0.15‰$ (V-SMOW) for the international NBS-28 (quartz) standard. The analyses were carried out using a Finnigan MAT 251 spectrometer at the Stable Isotope Laboratory, Estación Experimental del Zaidín (Granada, Spain).

5. Fluid inclusion data

5.1. Fluid inclusion petrography and chronology

Three types of fluid inclusion were identified in the quartz veins. They are all aqueous and no C–N–S species were detected by micro-Raman analysis (at G2R, Nancy, France). Notation of the fluid inclusion types follows the nomenclature of Boiron, Essarraj, Sellier, Cathelineau, Lespinasse, and Poty (1992), which takes into account the nature of the dominant chemical phases and the type of phase change. The relative chronology of the fluid inclusions is deduced from textural observations.

Lw1: idiomorphic inclusions (liquid + vapour) have been located as primary in the centre of the quartz crystals (QII) following growth planes parallel to the crystal faces (Fig. 2a). Some irregular inclusions have been recognised as pseudosecondary in fluid inclusion planes which

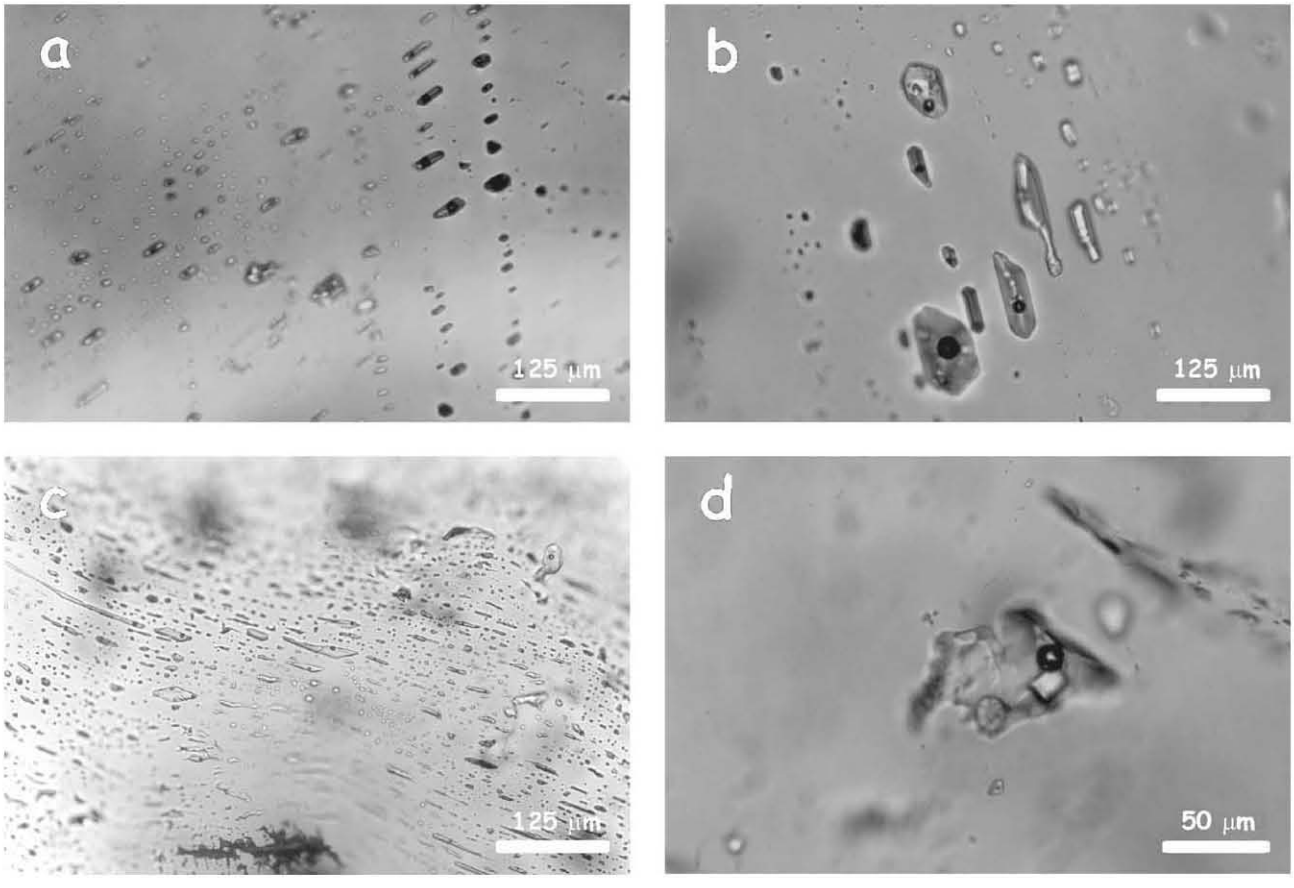

Fig. 2. (a) Primary Lw1 fluid inclusions following growth planes. (b) Primary Lw2 fluid inclusions. (c) Secondary Lw2 inclusions scattered along healed fractures. (d) Lw-h fluid inclusion showing a daughter cubic crystal (halite) and lamellar muscovite as trapped mineral.

Table 2
Fluid inclusion microthermometric data for barren quartz veins summarised by their host rock (granites and augen gneisses) (T_{FM}: first ice melting; T_{HH}: last hidrohalite melting; T_{MICE}: last ice melting; T_S: last solid melting; T_H: homogenization to liquid; [2] = number of samples; (970) = number of measurements)

Host rock	Granites			Augen gneisses
Locality	Colmenarejo [12], Cerceda [10], La Cabrera [4], Manzanares El Real [8]			Colmenarejo [7], Colmenar Viejo [3]
Inclusion type	Lw1	Lw2	Lw-h	Lw1
Components	H_2O–NaCl	H_2O–NaCl–$CaCl_2$	H_2O–$CaCl_2$–NaCl	H_2O–NaCl
Phases at room temperature	Two phases	Two phases	Three phases	Two phases
% Vapour	5–30	5–10	5–10	10–20
T_{FM} (°C) (30)	–	−67/−55, mode: −61	–	–
T_{HH} (°C) (215)	–	−18.2/−2, mode: −8	–	–
T_{MICE} (°C) (970)	−0.6/0 mode: −0.4	−26.7/−21.5, mode: −25	−47.5/−34, mode: −46	−0.1/0, mode: 0
T_S (°C) (110)	–	–	120/220 mode: 150	–
T_H (°C) (935)	140/300 mode: 250	70/160 mode: 120	60/160 mode: 130	140/300 mode: 260
Salinity	–	16/24 wt% NaCl 1/12 wt% $CaCl_2$	7/15 wt% NaCl 21/27 wt% $CaCl_2$	–
Bulk salinity (equiv. wt% NaCl)	0/1 mode: 0.6	24/27.3 mode: 26	30/38.1 mode: 37	0/0.2 mode: 0
NaCl/NaCl + $CaCl_2$	–	0.6/0.95	0.2/0.35	–

terminate abruptly within the crystal. Lw1 inclusions occur in all vein types.

Lw2: inclusions are primary and located in the margins of the crystals (QIII) (Fig. 2b). They can also be secondary, scattered along healed fractures in the centre of the crystals (QII) (Fig. 2c). They contain liquid + vapour at room temperature.

Lw-h: inclusions contain at least three phases (liquid + vapour + solid) at room temperature including a daughter crystal (Fig. 2d). They occur as pseudosecondary inclusions in QIII and, as trails of secondary inclusions cross-cutting Lw1 and Lw2 fluid inclusion populations. This inclusion type represents the last hydrothermal event in the barren quartz veins. Lw2 and Lw-h fluid inclusions are absent in the gneiss-hosted quartz veins.

5.2. Microthemometric results

Results are summarised in Table 2, together with all microthermometric abbreviations used in the text.

5.2.1. Lw1 inclusions

The first observable melting of ice takes place at around −25 °C. These eutectics are consistent with the interpretation of an aqueous solution belonging to the H_2O–NaCl system (Shepherd, Rankin, & Alderton, 1985). The T_{MICE} values (−0.6 to 0 °C; mode: −0.4) indicate low salinity, lower than 1 wt% NaCl. $T_{H\,L-V}$ are in the range of 140–300 °C, with 250 °C as the modal value (Fig. 3).

5.2.2. Lw2 inclusions

Values of T_{FM}, ranging from −67 to −55 °C (mode: −61 °C) and the brown-coloured character of crystals are both consistent with the presence of $CaCl_2$ in the fluid (Shepherd et al., 1985). However the temperatures are lower than the theoretical eutectic temperature in the H_2O–NaCl–$CaCl_2$ system, ~ −52 °C (Borisenko, 1977; Yanatieva, 1946). Such low T_{FM} values have been attributed to (i) a melting sequence according to the model univariant curve with a metastable eutectic point of around −70 °C (Davis, Lowenstein, & Spencer, 1990; Spencer, Moller, & Weare, 1990), and/or (ii) to the presence of additional components such LiCl (Zwart & Touret, 1994). Microthermometric analyses are based on measuring solid–liquid transition temperatures (T_{FM}, T_{MICE}, or T_{HH}). However, first-melting temperatures and identification of freezing-phases are indeed difficult to recognise, and are prone to error and misinterpretation. Raman spectra data from frozen solution in the system H_2O–NaCl–$CaCl_2$ indicate that at least some phase transitions between about −70 and −50 °C represent a crystallization event (hydrohalite and antarcticite crystallization) and not a metastable melting event (Samson & Walker, 2000). The demostrated existence of these crystallization events in natural fluid inclusions could lead unwarranted the interpretation of phase transitions below −50 °C (Samson & Walker, 2000).

Hydrohalite melting T_{HH} (−18.2 to −2 °C; mode: −8 °C) occurs after ice melting T_{MICE} (−26.7 to −21.5 °C; mode: −25 °C). The composition of these fluids has been calculated using an Excel-macro (Naden, 1996), and lies in the high salinity part of the H_2O–NaCl–$CaCl_2$ system, below the ice-hydrohalite cotectic curve around 16–24 wt% NaCl and 1–12 wt% $CaCl_2$. The bulk salinity ranges between 24 and 27.3 equiv. wt% NaCl (mode: 26 equiv. wt% NaCl). Lw2 inclusions homogenise to liquid and show lower temperatures (70–160 and 120 °C as the modal value) than the Lw1 fluids.

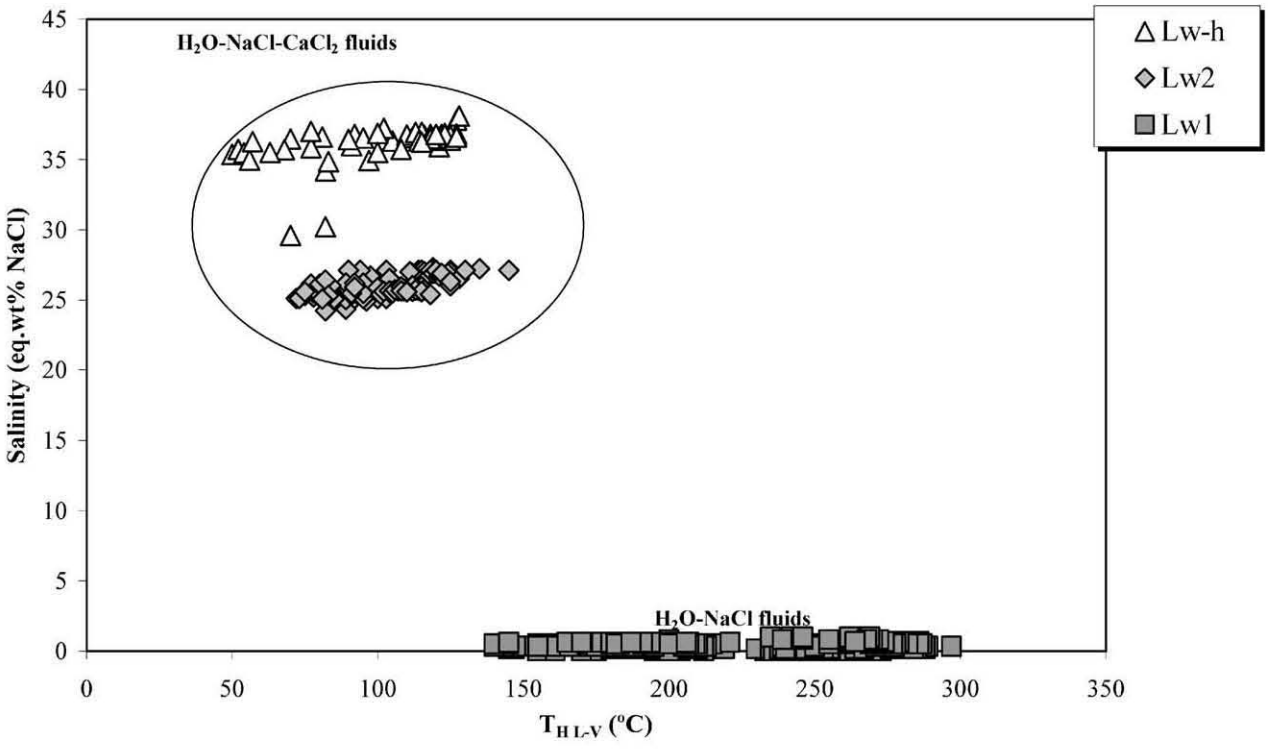

Fig. 3. $T_{H\,L-V}$ vs salinitity plot for Lw1, Lw2 and Lw-h fluid inclusions. Lw1 type display two populations showing $T_{H\,L-V}$ ranges between 140–220 and 230–300 °C.

5.2.3. Lw-h inclusions

These inclusions contain at least three phases at room temperature including a daughter halite crystal. The other solids are interpreted as trapped crystals because they do not dissolve or start to dissolve during heating, and are anomalously large compared to their host inclusions and constant liquid/solid volume ratios are not giving. Some of these have been identified as plagioclase and lamellar muscovite using SEM + EDS combining the morphology of the solids with qualitative chemical analysis. $T_{H\,L-V}$ homogenisation temperatures range from 60 to 160 °C (mode: 130 °C), and dissolution temperatures of halite from 120 to 220 °C (mode: 150 °C). An approximation to the high bulk salinity has been calculated for the Lw-h inclusions at between 30 and 38.1 equiv. wt% NaCl (mode: 37 equiv. wt% NaCl). The estimated compositions (calculated by a Microsoft Excel add-in, Naden, 1996) are 7–15 wt% NaCl and 21–27 wt% $CaCl_2$. Lw-h inclusions show dissolution temperatures of halite that are higher than homogenisation temperatures ($T_S > T_H$). It is likely that Lw-h inclusions have a possible mixture of additional components such as KCl, LiCl or H_2S (Zwart & Touret, 1994).

A T_H–salinity plot (Fig. 4a) indicates the presence of two fluids of different salinity but with a similar T_H range (70–140 °C). Lw2 inclusions are less saline than pseudo-secondary and secondary Lw-h inclusions, thus indicating a progression to higher salinity with quartz crystallization.

The Lw-h fluid is enriched in Ca relative to the Lw2 type (Fig. 4b). Slight differences in the NaCl/NaCl + $CaCl_2$ ratio can be observed between the different quartz veins. The La Cabrera vein, which is located in the northern part of the area, contains Lw2 inclusions with high NaCl/NaCl + $CaCl_2$ ratios; no Lw-h inclusions were observed. Lw2 fluid inclusions from Colmenarejo quartz veins, which are located in the southern part of the region, are more calcic. Inclusions from the other veins, Manzanares and Cerceda, show a wide range in Na/Ca rations and typically have lower T_H values.

5.3. Ion analyses

The atomic ratios Na/Ca and Na/Li were measured in Lw2 and Lw-h inclusions, however ratios in Lw1 inclusions could not be estimated due to their low salinity. Mole ratios for Lw2 inclusions are: Na/Ca = 7 and Na/Li = 14. Lw-h inclusions show an enrichment in Ca and Li (Na/Ca = 1.5, Na/Li = 3) with respect to Lw2 inclusion. These ratios confirm the presence of significant amounts of Li in Lw2 and Lw-h inclusions. Moreover, an enrichment in Li and Ca content is observed from the Lw2 to the Lw-h inclusions. Li concentrations have been measured in quartz crystals and range from 0 to 400 ppm.

Previously published data on bulk crush-leach analyses (Martín Crespo et al., 1999) are considered in this study. Samples chosen from the barren quartz veins for bulk chemical analysis of fluid inclusion leachates are characterised by a single inclusion type, representative of the higher salinity Lw2 fluids. The Cl/Br molar ratio (703 to 753) and

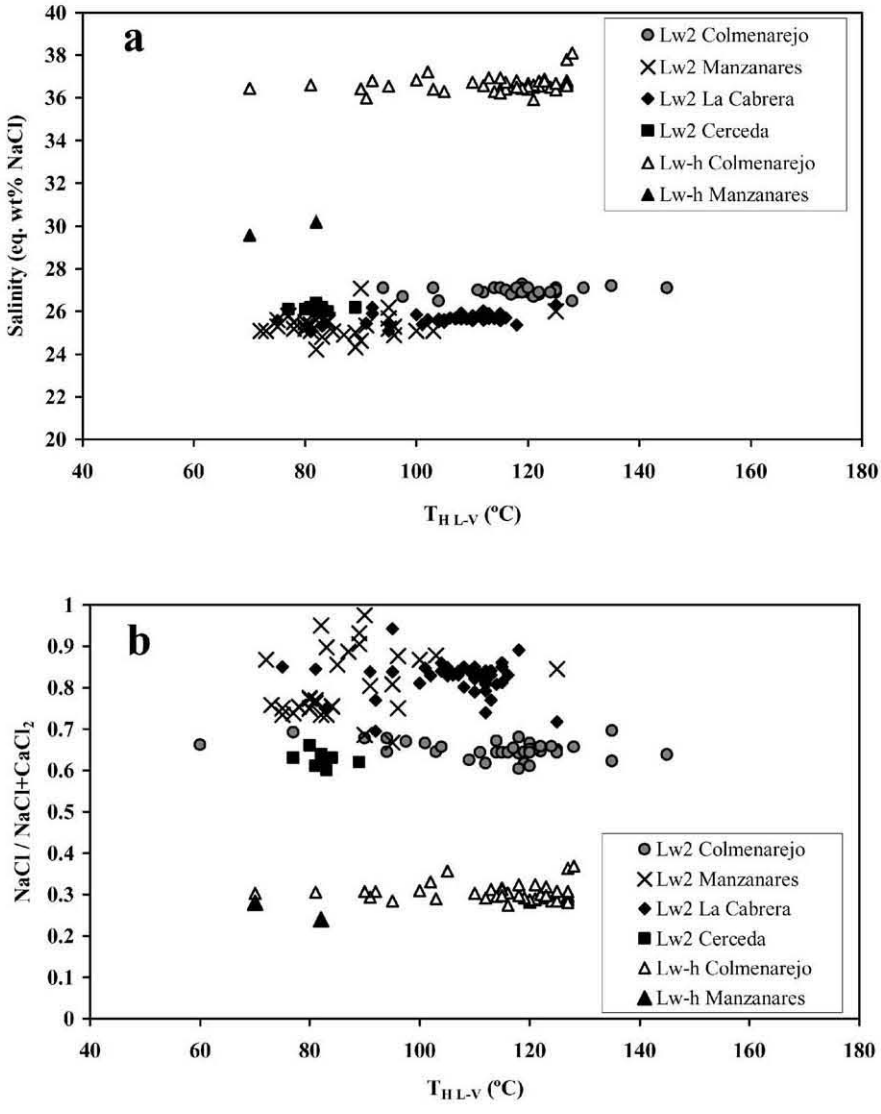

Fig. 4. Lw2 and Lw-h inclusions (H_2O–NaCl–$CaCl_2$). (a) $T_{H\,L\text{-}V}$ vs salinity plot. (b) $T_{H\,L\text{-}V}$ vs NaCl/NaCl + $CaCl_2$.

Na/Br molar ratio (508 to 1054) is close to the ratio for seawater (Cl/Br: 655 and Na/Br: 562, after Horita, Friedman, Lazar, & Holland, 1991), but slightly impoverished in Br.

6. *P–T* conditions

A reconstruction of the P–T conditions that prevailed during the entrapment of the fluids is given in Fig. 5.

The latest stage of quartz deposition is characterised by the circulation of H_2O–NaCl–$CaCl_2$ fluids. Since Lw2 and Lw-h inclusions show no evidence of boiling, and a mineral geothermometer is not available, fluid pressure is assumed to be greater than or equal to hydrosthatic pressure (P_h). Vuggy textures and the brittle nature of the host rock are taken as indicators of a hydrostatic pressure regime for this fluid. Maximum fluid pressures were constrained by the maximum depth of burial. Late Hercynian granites in the Spanish Central System were emplaced at depths of between 5 and 8 km, under a lithostatic pressure at ~2 kbar (Villaseca et al., 1998). If the pressure regime was entirely hydrostatic, a depth of 5 km indicates a P_{fluid} of less than 0.5 kbar. For this pressure range, the $CaCl_2$ bearing fluids were trapped at 70–140 °C (Fig. 5).

The early stage of hydrothermal circulation is characterised by a H_2O–NaCl fluid represented by low salinity inclusions. The mineral assemblage provides no additional constraints on the P–T conditions. Although T_H ranges between 140–220 and 230–300 °C, the most probable conditions for this stage are derived for modal isochores having T_H in the 230–300 °C range. The T_H range between 140 and 220 °C has been only measured in some fluid inclusions from the single quartz vein of the La Cabrera, and has not been considered representative data for P–T estimations. Trapping pressures are difficult to estimate precisely, but a maximum depth of 5 km suggests pressures <1 kbar, assuming a transition from lithostatic to hydrostatic pressure

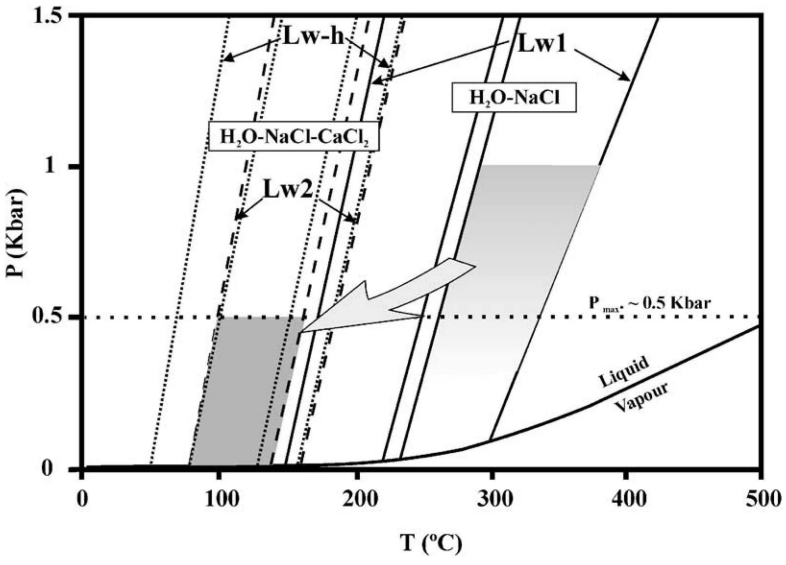

Fig. 5. Pressure–temperature diagram showing P–T constraints for different inclusion types. The isochores for the fluids have been drawn for each inclusion type: Lw1: solid lines; Lw2: dashed lines; Lw-h: dotted lines. The field for Lw1 inclusions (*light grey*) is determined by the isochores (modal range) and a assumed maximun $P_{fluid} \sim 1$ kbar. The field for Lw2 inclusions (*dark grey*) is determined by intersection of isochores (modal range), and calculated maximum P_{fluid} under hydrostatic regime.

regime during the earlier hydrothermal circulation stages. The overall fluid evolution shows a decreasing trend in the temperature and a progressive enrichment in NaCl and $CaCl_2$ content.

7. $^{39}Ar/^{40}Ar$ geochronology

To constrain the evolution of the fluids, hydrothermal muscovites from granite-hosted quartz veins (Colmenarejo) were analysed by the $^{39}Ar/^{40}Ar$ method. The spectrum obtained has a staircase shape (Fig. 6). A 'plateau' age of 274 ± 5 Ma is suggested by three of the four late steps between 45 and 95% fractional ^{39}Ar release. The steps with the lowest age could be explained by diffusion processes and by some post-crystallization heating, mainly at the border of the samples because of the later hydrothermal heating events. Several Mesozoic hydrothermal events have been recognised in the Spanish Central System, and Villa (1998) has shown that fluid–mineral interaction is more relevant for isotopic exchange compared to the thermal history of a mineral. Anyhow, the later hydrothermal

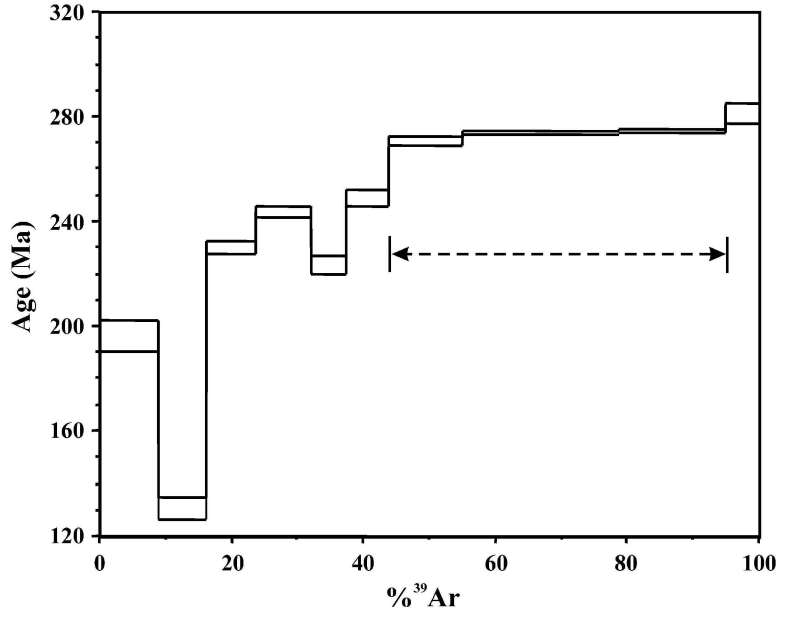

Fig. 6. Age spectrum of hydrothermal white mica. The spectrum obtained has a staircase shape and the 'plateau' is suggested by three of the four late steps.

Table 3
Stable isotope data. Measured (*Meas.*) fluid δD and $\delta^{18}O$ are bulk values for the total fluid inclusion population and quartz, respectively. Calculated (*Calc.*) fluid $\delta^{18}O$ values are derived from the bulk mineral data by means of fractionation factors at the appropriate temperature (Clayton et al., 1972) (N.D.: not determined)

Sample	Fluid type	Inclusion type	Minimum fluid trapping temperature (°C)[a]	Modal salinity of fluid inclusions (wt% NaCl equiv.)	*Meas.* quartz $\delta^{18}O_{SMOW}$ (‰)	*Calc.* quartz-fluid $\delta^{18}O_{SMOW}$ (‰)[b]	*Meas.* bulk fluid H_2O δD_{SMOW} (‰)
Col. G3	H_2O–NaCl	Lw1	170–295	0.4	6.8	−7/−1	(−105.5)[c]
Cer. G3		Lw1	140–290	1	8.1	−8/1	−55
Man.G1		Lw1	230–300	0.3	6.9	−7.3/1.5	−38/−59
Cab.G2		Lw1	140–230	0.5	10.6	−5.3/1.5	−71/−73.5
Col. M1		Lw1	140–260	0.15	7.6	−9/−1	−34.5/−64
Colv.M6		Lw1	140–290	0.15	9.7	−7/2	−45/−60
Col. G4	H_2O–NaCl–$CaCl_2$	Lw2	90–160	27	6.7	−20/−7.8	−116
Cer. G2		Lw2	75–90	26.2	N.D.	N.D.	N.D.
Man.G4		Lw2	70–115	25.5	8.5	−17/−6	−137
Cab.G1		Lw2	75–130	25.7	N.D.	N.D.	N.D.

[a] Fluid inclusions temperature range.
[b] Calculated using equations of Clayton et al. (1972) at the appropiate temperature.
[c] Anomalous data because of probably mixing with Lw2 inclusions.

temperatures have not raised the closure temperature for muscovites (Villa, 1998).

The age determined in the present study is higher than previously reported for sericite from phyllic alteration surrounding barren quartz veins, which was dated by the K–Ar method at 100 ± 4 Ma (Caballero et al., 1992). The large difference between the two ages suggests that two different hydrothermal events have been dated. The muscovite age determined in this work may correspond to the first hydrothermal stage. Alteration events around 270 Ma coincide with Permian extensional tectonics, and with a major hydrothermal phase in the Spanish Central System. The hydrothermal stage dated around 100 Ma corresponds to Lower Cretaceous, could be related to the later Ca-bearing fluids present in the barren quartz veins and considered as a younger reactivation of the faults.

8. Stable isotope results

The isotopic composition of the fluid have been measured (*Meas.*) for the δD values and calculated (*Calc.*) for the $\delta^{18}O$ values (Table 3).

The Lw1 fluid in granite-hosted veins shows a range of bulk δD (−70 to −38‰) and $\delta^{18}O$ (−8 to 1‰), comparable to values in gneiss-hosted veins (−64 to −34.5‰ for δD and −9 to 2‰ for $\delta^{18}O$). The low $\delta^{18}O$ values indicate a meteoric origin for the water, although the more positive values can be related to the interactions water–rocks (Fig. 7). An origin from seawater can be excluded since evaporated seawater will be close to halite saturation (~26.3 equiv. wt% NaCl; Holser, 1979), and the Lw1 fluid contains only 0.15–1 equiv. wt% NaCl.

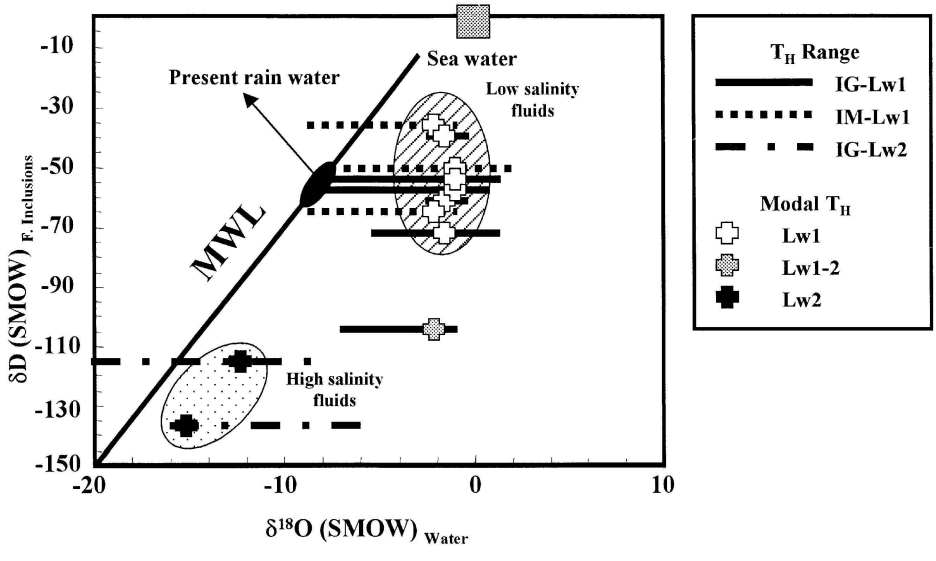

Fig. 7. $\delta^{18}O$–δD plot of Lw1 and Lw2 inclusions (GRH: granite-hosted veins, GNH: gneiss-hosted veins). Range in $\delta^{18}O$ corresponds to maximum and minimum trapped temperatures (Table 3).

The Lw2 fluid inclusions are only present in a granite-hosted quartz vein. The Lw2 fluid inclusion δD values cluster between -137 and -116‰ and δ^{18}O values between -20 and -6‰. The low δ^{18}O and δD range estimated for Lw2 fluid indicate a meteoric origin for the fluid. However, its high salinity (25.7–27 equiv. wt% NaCl) could indicate dissolution of evaporites. δD values are lower than those reported for other hydrothermal events involving meteoric fluids in the Spanish Central System (Tornos, Delgado, Casquet, & Galindo, 2000). Several possible origins for anomalously low δD values such as those reported here have been argued (Gleeson, Wilkinson, Boyce, Fallick, & Stuart, 1999): (i) water–organic matter interactions; (ii) contributions of hydrogen with different isotopic signature from mica trapped in fluid inclusions; (iii) post-entrapment hydrogen diffusion; and (iv) high-latitude and high-altitude meteoric precipitation. The first possibility can be ruled out because of the lack of organic matter. A source of hydrogen from micas and hydrogen diffusion could be considered. Trapped micas have been recognised in Lw1 and Lw2 fluid inclusions, however anomalously δD values in Lw1 fluid inclusions have not been recognised. Therefore, the contribution of hydrogen from trapped mica could be considered as negligible. Post-entrapment hydrogen diffusion from hosted quartz to fluid inclusion could be taken into account. Low δD values have been reported from quartz interstitial sites relative to molecular water, although the hydrogen isotope fractionation factors for the incorporation of hydrogen into quartz interstitial sites are unknown (Gleeson, Grant, & Roberts, 2000).

Anomalously low δD are often interpreted to indicate the involvement of high latitude/altitude meteoric waters in palaeoflow systems, which seems to be the main reason to explain such low δD values in Lw2 fluids.

Few data lie away from the isotopically well defined Lw1 group. These intermediate values between Lw1 and Lw2 δD data can be attributed to a mixture of Lw1 and Lw2 fluid inclusions. In the analysed sample the inclusions were not exclusively Lw1 and some Lw2 inclusions were also included.

9. Discussion

The early (Lw1) H_2O–NaCl fluid inclusions represent a high δD, δ^{18}O, high temperature and low salinity fluid consistent with an origin related to meteoric waters.

Fluids characterised as H_2O–NaCl have been recognised as being associated with earlier hydrothermal events of several age at the Sierra de Guadarrama: W–(Sn)–sulphide veins (García et al., 1999a; Vindel et al., 1995), epysienites (Caballero, 1993), As–(Ag) mineralizations (García et al., 1999b) and barite–fluorite (Pb–Zn) veins (Tornos et al., 1991). Therefore this type of fluid was present during all hydrothemal activity in the area.

The H_2O–NaCl–$CaCl_2$ fluids represent a late and minor event relative to the H_2O–NaCl fluids, and are restricted to granite-hosted veins. The absence of Ca-fluid inclusions in the gneiss-hosted quartz veins could be related to the hosted lithology. Foliation of gneisses could favour the fluid migration out of the veins. Stable isotope data indicate a meteoric origin for the H_2O–NaCl–$CaCl_2$ fluid, but the high salinity was probably derived from dissolution of evaporites. The age of the late fluid is $\leq$100 Ma, allowing the possibility that the fluid percolated through Triassic evaporites. Significant Mesozoic evaporitic basins are located in the northeast of the Spanish Central System (SCS) (Utrilla, Ortí, Pueyo, & Pierre, 1989; Utrilla, Pierre, Ortí, & Pueyo, 1992). The northern (Atlantic domain) and southern (Tethys domain) parts of the SCS were connected during the Cretaceous via NE–SW and NW–SE faults (Casas et al., 1998). Both sedimentary basins were palaeogeographically linked (Gil & García, 1996).

Li represent a good tracer of the evaporitic evolution of primary solutions. It behaves conservatively during seawater concentration and evaporite precipitation (Fontes & Matray, 1993). Significant Li concentrations in quartz crystals and in the H_2O–NaCl–$CaCl_2$ fluid were measured. High Li concentration have been typically reported from evaporitic sequences and attributed to highly concentrated brines (Fontes & Matray, 1993). Na/Br and Cl/Br ratios can be used to distinguish ions from different sources (Kesler et al., 1995). Halogens (Cl/Br and Na/Br ratios) from crush-leach analysis could represent their original seawater signature in a marine/evaporitic environment.

Moreover, the $CaCl_2$ content is also consistent with dissolution of evaporites, thus other Ca sources are not necessary. Sedimentary carbonates (higher δ^{18}O) and lower water–rock ratios are concordant with diagenetic water enriched in ^{18}O but not in D (Fig. 7).

It is important to stress that during Cretaceous time, this area was a low latitude (Ziegler, Scotese, & Barret, 1983). At present, the oxygen isotopic composition of meteoric water in latitudes between 0 and 20° is typified by values ranging between +1.5 and -7‰ (SMOW) (Rozanski, Araguás, & Gonfiantini, 1993). Ocean waters during the Mesozoic Era were between 2.3 and 1.2‰ lighter than at present (Scherer, 1977; Shackleton & Kennett, 1975). Therefore, a meteoric water derived from the evaporation of marine waters at that time could fall between -0.8 and -9.3‰ (SMOW). Even so, the measured (-137‰ $< \delta$D < -116‰) and calculated (-20‰ $< \delta^{18}$O < -6‰) isotopic composition of the fluids are too negative to be explained by differences in seawater composition. Most explanations for H_2O–NaCl–$CaCl_2$ fluids with anomalously low δD values are related to high-latitude and/or high altitude meteoric precipitation (Gleeson et al., 1999). However, palaeogeographic reconstructions of the Lower Cretaceous in this part of the Spanish Central System (Alonso, Floquet, Meléndez, & Salomón, 1982) indicate intermediate latitude close to the Cancer Tropic. Therefore, none of the previously

documented hypotheses for the formation of anomalously low δD fluids can adequately explain the occurrence of this type of fluids in the Spanish Central System during the Lower Cretaceous. However, other authors such as Dutta and Suttner (1986) and Marfil, Delgado, Rossi, La Iglesia, and Ramseyer (2000), studying kaolinites from this period, have also reported anomalously low isotopic values (compared to recent kaolinites that were formed in weathering profiles at low latitudes). A possible explanation could be the so called 'amount effect', that leads to more negative rain waters than expected at these latitudes (Fontes, 1980; Rozanski et al., 1993). At middle and lower latitudes, the isotopic content of precipitation is found to be higher in small amounts of rain but never near the poles. Highly depleted oxygen isotope values of actual and recent sediments indicate an origin related with wet periods characterised by intense tropical summer (monsoonal) rainfall with heavy thunderstorms (Luckge, Doose-Rolinski, Khan, Schulz, & Von Rad, 2001). Therefore, we should expect strong isotopic depletion in meteoric waters, such as those observed in modern areas with monsoonal climates (Feng, Cui, Tang, & Conkey, 1999; Marfil et al., 2000). Thus, periods of high precipitation and dissolution of evaporites may have promoted the formation of Lw2 fluids in equilibrium with very negative and high salinity waters. This data are concordant with the general climate of the Late Jurassic and Lower Cretaceous characterised by high atmospheric CO_2 levels and by a monsoonal rainfall pattern (Weissert & Mohr, 1996).

$CaCl_2$-rich brines with moderate to high salinity often occur around the margins of Mesozoic basins of central Europe, particularly in the vicinity of older granites (Heijlen, Muchez, Banks, & Nielsen, 2000; Lodemann et al., 1998; Muchez et al., 1995; Munoz et al., 1994; O'Reilly et al., 1997; Wilkinson et al., 1995), and have been related to the early north Atlantic rifting and associated to the Triassic–Jurassic evaporites (Halliday & Mitchell, 1984; Mitchell & Halliday, 1976; Munoz et al., 1999; O'Connor et al., 1993). Mineralizations can be spatially correlated to the granites formed by post-orogenic collapse in relation to intense fracturing. It is proposed that high salinity H_2O–$NaCl$–$CaCl_2$ solutions, that originated from residual evaporite brines and formation waters, infiltrated into the basement along extensional structures (Behr & Gerler, 1987; Behr, Reutel, Horn, & Van den Kerkhof, 1994, Reutel, Behr, Horn, Van den Kerkhof, 1994). Other models propose a fluid flow system involving meteoric water that increased in salinity because of interaction with evaporitic-bearing sequences, related to the Mesozoic extensional events (Muchez & Sintubin, 1998; Munoz et al., 1999). Fluid migration during Mesozoic time in the Spanish Central System belongs to a general history in the Variscan range, and can be compared to the model described in Munoz et al. (1999) for fluids related to major Mesozoic extensional events, coinciding with the opening of the Atlantic and Tethys oceans.

10. Conclusions

Barren quartz veins represent the latest event of the hydrothermal evolution in the Sierra de Guadarrama (Spanish Central System) and are characterised by two different fluids. The first fluid is represented by the H_2O–$NaCl$ system and characterised by low salinity. The isotopic data indicate a meteoric origin for this fluid. This early fluid is related to older hydrothermal events in the area: W–Sn–sulphide veins, episienites, As–Ag mineralizations and barite–fluorite veins. The youngest fluid belongs to the H_2O–$NaCl$–$CaCl_2$ system and has high salinity. Ca-brines have not been found in the older hydrothermal events in the Sierra de Guadarrama. This later fluid represents meteoric water salt-enriched by dissolution of Triassic evaporites. Palaeogeographic reconstructions of the Lower Cretaceous in this part of the Spanish Central System do not suggest low δD fluids commonly related to high-latitude and/or high-altitude. The most plausible explanation could be the 'amount effect', that leads to more negative rain waters than expected at tropical latitudes, such as those observed in monsoonal climates.

Fluid composition and evolution in barren quartz veins of the Spanish Central System are similar to other hydrothermal Post-Variscan events in central and south-western Europe. In all cases mineralization occurs around the margins of Mesozoic basins in the vicinity of granites and has been attributed to early Cretaceous Atlantic rifting. However, geochronological data suggest that several hydrothermal phases could be recorded in barren quartz veins up to Cretaceous. The first one (~270 Ma) is ubiquitous throughout the Spanish Central System, and represents a major hydrothermal circulation event, coincident with the Mid-Permian transition to extensional pre-rift tectonics. Other hydrothermal phases continued during the Mesozoic time until the Cretaceous. The late hydrothermal stage (~100 Ma) could be related to Ca-bearing fluids.

Acknowledgements

M. Christine Boiron (CREGU-G2R, Nancy, France) and I. Villa (Bern University, Switzerland) are thanked for comments and technical support with LIBS and geochronology analysis, respectively. R. Oyarzun is thanked for his careful reading and improvement of the English. TMC acknowledges post-graduate fellowship from the Comunidad de Madrid. The authors thank I. Samson and I.C. Scotchman for their helpful reviews.

References

Alonso, A., & Mas, J. R. (1982). Correlación y evolución paleogeográfica del Cretácico al norte y al sur del Sistema Central. *Cuadernos de Geología Ibérica*, *8*, 145–166.

Alonso, A., Floquet, M., Meléndez, A., & Salomón, J. (1982). *Cameros-Castilla, El Cretácico de España*. Madrid: Univ. Complutense pp. 345–456.

Behr, H. J., & Gerler, J. (1987). Inclusions of sedimentary brines in Post-Variscan mineralizations in the Federal Republic of Germany—A study by neutron activation analysis. *Chemical Geology*, *61*, 65–77.

Behr, H. J., Horn, E. E., Frentzel-Beyme, K., & Reutel, Ch. r. (1987). Fluid inclusion characteristic of the Variscan and Post-Variscan mineralizing fluids in the Federal Republic of Germany. *Chemical Geology*, *61*, 273–285.

Behr, H. J., Reutel, Ch. r., Horn, E. E., & Van den Kerkhof, A. M. (1994). The fluid research program of the Continental Deep Drilling Project KTB (Germany). II. Ca–Na–Cl basement brines as tracers of fluid activity and mineralization in an orogenic collapse system. *PACROFI V, Cuernavaca*, 8.

Bellido, F., Capote, R., Casquet, C., Fúster, J. M., Navidad, M., Peinado, M., & Villaseca, C. (1981). Caracteres generales del cinturón hercínico en el sector oriental del Sistema Central Español. *Cuadernos de Geología Ibérica*, *7*, 15–51.

Bodnar, R. J. (1993). Revised equation and table for determining the freezing point depression of H_2O–NaCl solutions. *Geochimica et Cosmochimica Acta*, *57*, 683–684.

Boiron, M. C., Dubessy, J., André, N., Briand, A., Lacour, J. L., Mauchien, P., & Mermet, J. M. (1991). Analysis of mono-atomic ions in individual fluid inclusions by laser-produced plasma emission spectroscopy. *Geochimica et Cosmochimica Acta*, *55*, 917–923.

Boiron, M. C., Essarraj, S., Sellier, E., Cathelineau, M., Lespinasse, M., & Poty, B. (1992). Identification of fluid inclusions in relation to their host microstructural domains in quartz by cathodoluminescence. *Geochimica et Cosmochimica Acta*, *56*, 175–185.

Boiron, M. C., Moissette, A., Fabre, C., Dubessy, J., Banks, D., & Yardley, B. W. (1997). Ion analysis in individual fluid inclusions by Laser Ablation-Optical Emission Spectroscopy. Application to natural fluid inclusions. *Proceedings of the XIV ECROFI Conference, Nancy*, 44.

Borisenko, A. S. (1977). Study of the salt composition of solutions in gas–liquid inclusions in minerals by the cryometric method. *Soviet Geology and Geophysics*, *18*, 11–19.

Borthwick, J., & Harmon, R. (1982). A note regarding ClF_3 as an alternative to BrF_5 for oxygen from oxygen isotope analysis. *Geochimica et Cosmochimica Acta*, *46*, 1665–1668.

Bottrell, S. H., Yardley, B. W. D., & Buckley, F. B. (1988). A modified crush-leach method for the analysis of fluid inclusion electrolytes. *Bulletin of Mineralogy*, *111*, 279–290.

Caballero, J. M., Casquet, C., Galindo, C., Gonzalez-Casado, J. M., Snelling, N., & Tornos, F. (1992). Dating of hidrothermal events in the Sierra de Guadarrama, Iberian Hercynian Belt, Spain. *Geogaceta*, *11*, 18–22.

Caballero, J. M., (1993). Las episienitas de la Sierra de Guadarrama: un caso singular de alteración hidrotermal de edad post-hercínica. *PhD Thesis*. Complutense University, Madrid.

Canals, A., & Cardellach, E. (1993). Strontium and sulphur isotope geochemistry of low-temperature barite–fluorite veins of the Catalonian Coastal Range (NE Spain): A fluid mixing model and age constraints. *Chemical Geology*, *104*, 269–280.

Casas, A., Cortés, A. L., Liesa, C., Soria, A. R., Terrinha, P., Kullberg, J. C., & da Rocha, R. (1998). Estudio comparado de la evolución e inversión de distintas cuencas mesozoicas de la Placa Ibérica. *Geogaceta*, *24*, 67–70.

Casillas, R., Vialette, Y., Peinado, M., Duthou, J. L., & Pin, C. (1991). Ages et caracteristiques isotopiques (Sr–Nd) des granitoides de la Sierra de Guadarrama occidentale (Espagne). In R. Black, B. Bonin, A. Giret & P. Sabate, *Granites oceaniques et continentaux*.

Charef, A., & Sheppard, S. M. F. (1988). The Malines Cambrian carbonate shale-hosted Pb–Zn deposit, France: Thermometric and isotopic (H, O) evidence for pulsating hydrothermal mineralization. *Mineralium Deposita*, *23*, 86–95.

Clayton, R. N., & Mayeda, T. K. (1963). The use of bromine pentafluoride in the extraction of oxygen from oxides and silicates for isotopic analysis. *Geochimica et Cosmochimica Acta*, *27*, 43–52.

Clayton, R. N., O'Neil, J. R., & Mayeda, T. K. (1972). Oxygen isotope exchange between quartz and water. *Journal of Geophysical Research*, *77*, 3057–3067.

Davis, D. W., Lowenstein, T. K., & Spencer, R. J. (1990). Melting behavior of fluid inclusions in laboratory-grown halite crystals in the systems NaCl–H_2O, NaCl–KCl–H_2O, NaCl–$MgCl_2$–H_2O, and NaCl–$CaCl_2$–H_2O. *Geochimica et Cosmochimica Acta*, *54*, 591–601.

Dutta, P. K., & Suttner, L. J. (1986). Alluvial sandstone composition and paleoclimate. II. Authigenic mineralogy. *Journal of Sedimentary Petrology*, *56*, 346–358.

Fabre, C., Boiron, M. C., Dubessy, J., & Moissette, A. (1999). Determination of ions in individual fluid inclusions by laser ablation optical emission spectroscopy: Development and applications to natural fluid inclusions. *Journal of Analytical Atomic Spectrometry*, *14*, 913–922.

Feng, X. H., Cui, H. T., Tang, K. L., & Conkey, L. E. (1999). Tree-ring delta D as an indicator of Asian monsoon intensity. *Quaternary Research*, *51*, 262–266.

Fontes, J. Ch. (1980). Environmental isotopes in groundwater hydrology. In P. Fritz & J. Ch. Fontes, *Handbook of environmental isotope geochemistry. The terrestrial environment* (pp. 75–140). .

Fontes, J. Ch., & Matray, J. M. (1993). Geochemistry and origin of formation brines from the Paris Basin, France. 1. Brines associated with Triassic salts. *Chemical Geology*, *109*, 149–175.

Galindo, C., Tornos, F., Darbyshire, D. P. F., & Casquet, C. (1994). The age and origin of the barite–fluorite (Pb–Zn) veins of the Sierra de Guadarrama (Spanish Central System, Spain): a radiogenic (Nd, Sr) and stable isotope study. *Chemical Geology*, *112*, 351–364.

García, E., Vindel, E., & López García, J. A. (1999a). Análisis de la geometría de la circulación hidrotermal en granitos mineralizados del área de San Rafael (Sistema Central Español). *Reviews in Sociedad Geológica de España*, *12*, 369–376.

García, E., Vindel, E., & López García, J. A. (1999b). Evolución de los fluidos asociados a la mineralización de As–(Ag) de Bustarviejo (Sistema Central): Estudio preliminar. *Bolivian Sociedad Española de Mineralogía*, *22*, 49–50.

Gil, J., & García, A. (1996). El Cretácico del borde meridional del Sistema Central: unidades litoestratigráficas y secuencias deposicionales. *Estudios Geológicos*, *52*, 37–49.

Gleeson, S. A., Wilkinson, J. J., Boyce, A. J., Fallick, A. E., & Stuart, F. M. (1999). On the occurrence and wider implications of anomalously low δD fluids in quartz veins, South Cornwall, England. *Chemical Geology*, *160*, 161–173.

Gleeson, S. A., Grant, K., & Roberts, S. (2000). Fluid inclusion δD in quartz does not always indicate the source of palaeo-hydrothermal fluids. *Journal of Conference Abstracts*, *5* (2), 445.

Godfrey, J. D. (1962). The deuterium content of hidrous minerals from the East-Central Sierra Nevada and Yosemite National Park. *Geochimica et Cosmochimica Acta*, *26*, 1215–1245.

Halliday, A. N., & Mitchell, J. G. (1984). K–Ar ages of clay-size concentrates from the mineralization of the Pedroches Batholith, Spain, and evidence for Mesozoic hydrothermal activity associated with the break up of Pangaea. *Earth and Planetary Science Letters*, *68*, 229–239.

Heijlen, W., Muchez, Ph., Banks, D., & Nielsen, P. (2000). Origin and geochemical evolution of synsedimentary, syn- and post-tectonic high-salinity fluids at the Variscan thrust front in Belgium. *Journal of Geochemical Exploration*, *69–70*, 149–152.

Holser, W. (1979). Trace elements and isotopes in evaporites. R. G. Burns. *Marine Minerals, Reviews in mineralogy*, *6*, 295–346.

Horita, J., Friedman, T. J., Lazar, B., & Holland, H. D. (1991). The composition of Permian seawater. *Geochimica et Cosmochimica Acta*, *55*, 417–432.

Ibarrola, E., Villaseca, C., Vialette, Y., Fúster, J. M., Navidad, M., Peinado, M., & Casquet, C. (1987). *Dating of Hercynian granites in the Sierra de Guadarrama (Spanish Central System)*, *Geología de los*

granitoides y roca asociadas del Macizo Hespérico. Madrid: Rueda pp. 377–383.

Kamber, B. S., Blenkinsop, T. G., Villa, I. M., & Dahl, P. S. (1995). Proterozoic transpressive deformation in the Northern Marginal Zone, Limpopo Belt, Zimbabwe. *Journal of Geology*, *103*, 493–508.

Kesler, S. E., Appold, M. S., Martini, A. M., Walter, L. M., Huston, T. J., & Kyle, J. R. (1995). Na–Cl–Br systematics of mineralizing brines in Mississippi Valley-type deposits. *Geology*, *23*, 641–644.

Lodemann, M., Fritz, P., Wolf, M., Ivanovich, M., Hansen, B. T., & Nolte, E. (1998). On the origin of saline fluids in the KTB (Continental Deep Drilling Project of Germany). *Applied Geochemistry*, *13*, 653–671.

Luckge, A., Doose-Rolinski, H., Khan, A. A., Schulz, H., & Von Rad, U. (2001). Monsoonal variability in the northeastern Arabian Sea during the past 5000 years: Geochemical evidence from laminated sediments. *Palaeogeography, Palaeoclimatology and Palaeoecology*, *167*, 273–286.

MacDonald, A. J., & Spooner, T. C. (1981). Calibration of a Linkam TH 600 programmable heating–cooling stage for microthermometric examination of fluid inclusions. *Economic Geology*, *76*, 1248–1258.

Marfil, R., Delgado, A., Rossi, C., La Iglesia, A., & Ramseyer, K. (2002). Origin and diagenetic evolution of kaolin minerals in reservoir sandstones and associated shales of the Jurassic and Cretaceous of the Salam Field, Western Desert (Egypt). *The Clay Cement Special Publication, International Association of Sedimentologists*, in press.

Martín Crespo, T., López García, J. A., Banks, D., Vindel, E., & García, E. (1999). Hydrothermal fluids in barren quartz veins (Spanish Central System). A comparison with W (Sn) and F (Ba) veins. *Bolivian Sociedad Española de Mineralogía*, *22*, 83–94.

Mitchell, J. G., & Halliday, A. N. (1976). Extent of Triassic/Jurassic hydrothermal ore deposits on the North Atlantic margins. *Transactions of Institute of Mineral Metallurgy*, *B85*, 159–161.

Moissette, A., Dubessy, J., Boiron, M. C., Fabre, C., Mauchien, P., & Lacour, J. L. (1997). Laser ablation OES and its application to individual fluid inclusions analysis: State of the art. *Proceedings of the XIV ECROFI, Nancy*, 211–212.

Muchez, Ph., & Sintubin, M. (1998). Contrasting origin of palaeofluids in a strike–slip fault system. *Chemical Geology*, *145*, 105–114.

Muchez, Ph., Slobodnik, M., Viaene, W. A., & Keppens, E. (1995). Geochimical constraints on the origin and migration of palaeofluids at the northern margin of the Variscan foreland, southern Belgium. *Sedimentary Geology*, *96*, 191–200.

Munoz, M., Boyce, A. J., Courjault-Rade, P., Fallick, A. E., & Tollon, F. (1994). Multi-stage fluid incursion in the Palaeozoic basement-hosted Saint-Salvy ore deposit (NW Montagne Noire, Southern France). *Applied Geochemistry*, *9*, 609–626.

Munoz, M., Boyce, A. J., Courjault-Rade, P., Fallick, A. E., & Tollon, F. (1999). Continental basinal origin of ore fluids from southwestern Massif central fluorite veins (Albigeois, France): evidence from fluid inclusion and stable isotope analyses. *Applied Geochemistry*, *14*, 447–458.

Naden, J. (1996). CalcicBrine: a Microsoft Excel 5.0 Add-in for calculating salinities from microthermometric data in the system NaCl–$CaCl_2$–H_2O. *Program and Abstracts PACROFI VI, Wisconsin*, *1996*, 97–98.

O'Connor, P. J., Högelsberger, H., Feely, M., & Rex, D. C. (1993). Fluid inclusion studies, rare-earth element chemistry and age of hydrothermal fluorite mineralization in western Ireland—A link with continental rifting? *Transactions of Institute of Mineral Metallurgy*, *B102*, 141–148.

O'Reilly, C., Jenkin, G. R. T., Feely, M., Alderton, D. H. M., & Fallick, A. E. (1997). A fluid inclusion and stable isotope study of 200 Ma of fluid evolution in the Galway Granite, Connemara, Ireland. *Contributions of Mineralogy and Petrology*, *129*, 120–142.

Pérez del Villar, L., Crespo, M. T., Pardillo, J., Pelayo, M., & Galán, M. P. (1996a). U and Th series disequilibrium in the unaltered and hydrothermally altered granites from the El Berrocal site. *Applied Radiation Isotopes*, *47*, 1115–1119.

Pérez del Villar, L., De la Cruz, B., Pardillo, J., Cózar, J. S., Pelayo, M., Marín, C., Rivas, P., Reyes, E., Caballero, E., Delgado, A., Núñez, R., Crespo, M. T., & Galán, M. P. (1996b). *Lithogeochemical characterization and evolutive model of the El Berrocal site: analogies with a HLRWR. Topical Report 2, El Berrocal project. Characterization and validation of natural radionuclide migration processes under real conditions on the fissured granitic environment*, vol. 1. ENRESA pp. 302–487.

Reutel, Chr., Behr, H. J., Horn, E. E., & Van den Kerkhof, A. M. (1994). The fluid research program of the Continental Deep Drilling Project KTB (Germany): I. Characteristics of fluid inclusions and their relationship with saline water and gases in crystalline rocks. *PACROFI V, Cuernavaca*, *1994*, 80.

Rozanski, K., Araguás, L., & Gonfiantini, R. (1993). Isotopic patterns in modern global precipitation. *Climatic Change in Continental Isotopic Records, Geophysical Monograph*, *78*, 1–36.

Samson, I. M., & Walker, R. T. (2000). Cryogenic raman spectroscopic studies in the system NaCl–$CaCl_2$–H_2O and amplications for low-temperature phase behaviour in aqueous fluid inclusions. *Canadian Mineralogist*, *38*, 35–43.

Scherer, M. (1977). Preservation, alteration and multiple cementation of aragonite skeletons from the Cassian beds (U. Triassic, Southern Alps): Petrographic and geochemical evidence. *Neues Jahrbuch fur Geologie und Palaontologie*, *154*, 213–262.

Shackleton, N. J., & Kennett, J. (1975). Paleotemperature history of the Cenozoic and the initiation of the Antarctic glaciation: Oxygen and carbon isotope analyses in DSDP Sites 227, 279 and 281. *Initial Reports of the Deep Sea Drilling Project*, *29*, 743–755.

Shepherd, T. J., Rankin, A. H., & Alderton, D. H. M. (1985). *A Practical Guide to Fluid Inclusion Studies*, London: Blackie and Sons.

Spencer, R. J., Moller, N., & Weare, J. H. (1990). The prediction of mineral solubilities in natural waters: A chemical equilibrium model for the Na–K–Ca–Mg–Cl–SO_4–H_2O system at temperatures below 25 °C. *Geochimica et Cosmochimica Acta*, *54*, 575–590.

Tornos, F., Casquet, C., Locutura, J., & Collado, R. (1991). Fluid inclusion and geochemical evidence for fluid mixing in the genesis of Ba–F (Pb–Zn) lodes of the Spanish Central System. *Mineralogical Magazine*, *55*, 225–234.

Tornos, F., Delgado, A., Casquet, C., & Galindo, C. (2000). 300 Million years of episodic hydrothermal activity: Stable isotope evidence from hydrothermal rocks of the Eastern Iberian Central System. *Mineralium Deposita*, *35*, 551–569.

Utrilla, R., Ortí, F., Pueyo, J. J., & Pierre, C. (1989). Stable isotope study of Mesozoic and Cenozoic evaporitic formations from Spain. *European Union Geoscience, Strasbourg*, *1*, 335.

Utrilla, R., Pierre, C., Ortí, F., & Pueyo, J. J. (1992). Oxygen and sulphur isotope composition as indicators of the origin of Mesozoic and Cenozoic evaporites from Spain. *Chemical Geology*, *102*, 229–244.

Vennemann, T., & Smith, H. (1990). The rate and temperature of reaction of ClF_3 with silicate minerals and their relevance to oxygen isotope analysis. *Chemical Geology*, *86*, 83–88.

Vialette, Y., Bellido, F., Fúster, J. M., & Ibarrola, E. (1981). Datos geocronológicos sobre el granito de La Cabrera. *Cuadernos Geología Ibérica*, *7*, 327–338.

Villa, I. M. (1998). Isotopic closure. *Terra Nova*, *10*, 42–47.

Villaseca, C., Eugercios, L., Snelling, N. J., Huertas, M. J., & Castellón, T. (1995). Nuevos datos geocronológicos (Rb–Sr, K–Ar) de granitoides hercínicos de la Sierra de Guadarrama. *Reviews in Sociedad Geológica de España*, *8*, 129–140.

Villaseca, C., Barbero, L., & Rodgers, G. (1998). Crustal origin of Hercynian peraluminous granitic batholiths of Central Spain: Petrological, geochemical and isotopic (Sr, Nd) constraints. *Lithos*, *43*, 55–79.

Vindel, E., Lopez, J. A., Boiron, M. C., Cathelineau, M., & Prieto, A. C. (1995). P–V–T–X–fO_2 evolution from wolframite to sulphide depositional stages in intragranitic W-veins. An example from the Spanish Central System. *European Journal of Mineralogy*, *7*, 655–673.

Vindel, E., Lopez, J. A., Martín Crespo, T., & García, E. (2000). Fluid

evolution and hydrothermal processes of the Spanish Central System. *Journal of Geochemical Exploration*, *69–70*, 359–362.

Weissert, H., & Mohr, H. (1996). Late Jurassic climate and its impact on carbon cycling. *Palaeogeography, Palaeoclimatology and Palaeoecology*, *122*, 27–43.

Wilkinson, J. J., Jenkin, G. R. T., Fallick, A. E., & Foster, R. P. (1995). Oxygen and hydrogen isotopic evolution of Variscan crustal fluids, south Cornwall, UK. *Chemical Geology*, *123*, 239–254.

Yanatieva, O. K. (1946). Polytherms of solubility of salts in the tropic system $CaCl_2$–$MgCl_2$–H_2O and $CaCl_2$–NaCl–H_2O. *Journal of Applied Chemistry*, *19*, 709–722.

Yardley, B. W. D., Banks, D. A., Bottrell, S. H., & Diamond, L. W. (1993). Post-metamorphic gold–quartz veins from N.W. Italy: The composition and origin of the ore fluid. *Mineralogical Magazine*, *57*, 407–422.

Zhang, Y., & Frantz, D. (1987). Determination of the homogenisation temperatures and densities of supercritical fluids in the system NaCl–KCl–$CaCl_2$–H_2O using synthetic fluid inclusions. *Chemical Geology*, *64*, 335–350.

Ziegler, A. M., Scotese, C. R., & Barret, S. F. (1983). *Mesozoic and Cenozoic paleogeographic maps, Tidal friction and the earth's rotation II*. Berlin: Springer pp. 240–252.

Zwart, E. W., & Touret, J. L. R. (1994). Melting behaviour and composition of aqueous fluid inclusions in fluorite and calcite: Applications within the system H_2O–$CaCl_2$–NaCl. *European Journal of Mineralogy*, *6*, 773–786.